Acta Scientiarum
http://periodicos.uem.br/ojs
ISSN on-line: 1807-8664
Doi: 10.4025/actascitechnol.v46i1.64257

Meta-structure based on coupled resonators for low-frequency broadband sound absorption

Lucas Adelmo Santos, Gildean do Nascimento Almeida*, Erasmo Felipe Vergara, Leandro Rodrigues Barbosa and Linconl César Bastos Farias

Laboratório de Vibrações e Acústica, Departamento de Engenharia Mecânica, Universidade Federal de Santa Catarina, Bairro Trindade, 88040-900, Florianópolis, Santa Catarina, Brazil. *Author for correspondence. E-mail: gildean_fsa@hotmail.com

ABSTRACT. This work investigates and explains the behavior of an acoustic meta-structure based on different coupled Helmholtz resonators (HR). The analytical formulation of the Maa model is used to represent both the acoustic impedance and the sound absorption mechanism of the absorber. The structures are numerically modeled using finite element method and validated experimentally in an impedance tube considering sound waves of normal incidence. The absorber samples were manufactured in ABS (acrylonitrile butadiene styrene) polymer material with the additive manufacturing technique by extrusion of material. The results of the impedance tube, numerical and theoretical tests showed agreement and the sound absorber showed a sub-wavelength scale with perfect sound absorption ($\alpha \geq 0.97$) and broadband of 292 Hz in the low frequency region (200 - 600 Hz). We deduced that the excellent experimental result obtained is due to the high resolution used in the sample manufacturing ($\pm$ 0.1 mm) which minimized manufacture errors. Finally, the influences of the main parameters of the HR panel (width and depth of the micro-slit) on the sound absorption coefficient of the absorber were also analyzed.

Keywords: micro-slit; low-frequency sound absorption; additive manufacturing; Helmholtz resonators.

Received on July 5, 2022.
Accepted on July 3 2023.

Introduction

Sound absorption is a challenging for the scientific community, especially with regard to broadband low-frequency sound absorption. In recent decades, efforts dedicated to the study of the subject have always been highlighted. Designing a perfect low-frequency acoustic absorbers is challenging especially when the structure must have sub-wavelength thickness.

This interest is motivated by the wide applicability that these absorbers allow, for example in noise and vibrations control, acoustic insulation in the entire frequency spectrum, innovative acoustic solutions in the industrial field, among others. For this purpose, the advancement of acoustic metamaterials has motivated a series of absorber designs based on: locally resonant elements (Groby et al, 2015; Romero-Garcia et al, 2016; Wei, Zhigang, Linyong, & Xiaopeng, 2021), membrane resonators (Yang et al, 2015; Ma, Yang, Xiao, Yang, & Sheng, 2014; Mei et al, 2012), Fabry-Pérot (FP) type channels (Wu et al, 2019; Wang, Zhao, Yang, Zhong, & Wen, 2018, Almeida, Vergara, Barbosa, Lenzi, & Birch, 2021a) and symmetrical coiled up spaces (Almeida, Vergara, Barbosa, & Brum, 2021b; Almeida, Vergara, Barbosa, Lenzi, & Birch, 2021c).

Acoustic metamaterials (AMM) or meta-structures (MS) are absorbers that consist of periodic structures that repeat the so-called unit cell (UC), whose geometry is designed based on the objective to be achieved. These absorbers carry out the ability to manipulate and control sound waves with dimensions much greater than the material itself, employing the effect of local resonance. It allows them to be created with a much finer structure than conventional porous materials (e.g., cellular, fibrous and granular) or microperforated panels (MPP), therefore they offer new solutions to control noise problems.

Junfei, Wenqi, Yangbo, Bogdan-Ion, and Steven (2016) proposed a metasurface acoustic (MSA) with subwavelength scale where 99% sound absorption was reached experimentally at 511 Hz based on the coupling of different resonators and the hybrid resonance mode. On the other hand, Zhao, Wang, Wen, Lam, and Umnova (2018) presented the analytical formulation of the model, and through the numerical simulations and experiments they obtained good sound absorption in the range of 700-1200 Hz. Although these and others studies are successful (Xie, Li, Yan, & Yang, 2022; Han, Ji, & Qiu, 2021; Liu, Wu, & Ma, 2021), further research on low-frequency broadband sound absorption in the range 200-600 Hz is necessary.

In this work, unlike the studies mentioned above, we design the coupling of different resonators and based on the hybrid resonance mode, we guarantee low-frequency and broadband sound absorption with the absorber structure presenting subwavelength scale. Analytical method and numerical simulations using finite element model (FEM) are detailed. Furthermore, samples are manufactured using 3D-printing technology for experimental evaluation in an impedance tube for normal incidence of sound waves.

Material and methods

In Figure 1, the details of the meta-structure (MS) with two resonators (A and B) coupled with their respective geometric parameters are show in the xy plane. It can be seen that the micro-slit is located in the geometric center of the panel, arranged along in the x direction and coupled to the air cavity.

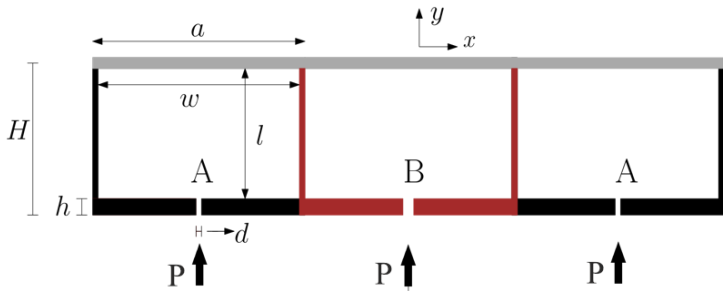

Figure 1. MS structure with two different HRs coupled. The total thickness of the structure is H, the width and depth of the micro-slit are d and h, respectively. The rear cavity of the micro-slit has width w, length and height l.

Theoretical method

Plane waves of amplitude P are concentrated on the MS panel along the y direction. The solution of the wave equation of air movement in the micro-slit for an axial velocity is obtained by (Maa, 2000)

$$-\frac{\partial P}{\partial y} = j\omega\rho_0 u - \eta \frac{\partial^2 u}{\partial x^2}, \quad (1)$$

where u is the particle velocity along y direction, $\rho_0 = 1.21$ kg m^{-3} is the air density, $\eta = 1.8134\ x\ 10^{-5}$ Pa.s is the dynamic viscosity and $\omega = 2\pi f\ is$ the angular frequency. Considering that air is incompressible and being the micro-slit depth much less than the wavelength, the term $\partial P/\partial y$ in the Equation (1) can be replaced by $\Delta P/\ h$, with ΔP representing the sound pressure variation between the ends of the micro-slit. Solving Equation (1) for u and the ratio of ΔP for the average value of u over the cross-sectional area of the micro-slit, we obtain the acoustic impedance of the panel containing the micro-slit according to perforation pattern

$$\tilde{Z}_p = \frac{\Delta P}{\bar{u}} = \frac{j\omega\rho_0 h}{\Theta}\left[1 - \frac{\tanh(\sigma\sqrt{j})}{\sigma\sqrt{j}}\right]^{-1}, \quad (2)$$

where $\Theta = (S_f/S_0)$ is the porosity of the unit cell, $S_f = wd$ is the cross-sectional of the micro-slit, h is the thickness of the perforation and $\sigma = d\sqrt{\rho_0\omega/4\eta}$ is the ratio of the gap diameter and layer thickness boundary layer or constant perforation. It is also necessary to add the corrections of the micro-slit, so the air movement on the face of the panel will be compressed in the micro-slit, as its volume is small, inducing an additional resistance, i.e., $\sqrt{2\rho_0\eta\omega}/(2\Theta)$ (Cobo & Simón, 2019). Moreover , based on Rayleigh′s derivation for an elliptic opening and using the elliptic integral of the first species (Maa, 2000), a final correction for the reactance needs to be defined due to sound radiation at both ends of the slit (Zhao et al., 2018), i.e., $(j\omega\rho_0 dF_e)/(2F(\varepsilon)\Theta)$, where $F(\varepsilon) = [1 - 1.4\varepsilon + 0.338\varepsilon^3 + 0.0679\varepsilon^5 \cdots]^{-1}$ is the Fok correction function due to the interaction of air radiation (Cobo, Colina, & Simón, 2020), $\varepsilon = d/l$, and F_e denotes the complete elliptic integral in which an appropriately shaped ellipse approaches the slit and is obtained by (Maa, 2000)

$$F_e = \int_0^{\frac{\pi}{2}} \frac{d\theta}{\sqrt{1-e^2(\sin\theta)^2}} = \frac{\pi}{2}\left\{\left(\frac{1}{2}\right)^2 e^2 + \left(\frac{3}{8}\right)^2 e^4 + \left(\frac{15}{48}\right)^2 e^6 + \cdots\right\}, \quad (3)$$

where $e = \sqrt{1-(d/L)^2}$ is the eccentricity of the ellipse. Thus, the exact impedance of the panel with a micro-slit and its final corrections is obtained by

$$\tilde{Z}_p = \frac{\Delta P}{\bar{u}} = \frac{j\omega\rho_0 h}{\Theta}\left[1 - \frac{\tanh(\sigma\sqrt{j})}{\sigma\sqrt{j}}\right]^{-1} + \frac{\sqrt{2\rho_0\eta\omega}}{2\Theta} + \frac{j\omega\rho_0 F_e\, d}{2F(\varepsilon)\Theta}. \quad (4)$$

The rigid back cavity of the MS can be considered as an addition to the special reactance by

$$\tilde{Z}_c = -j\frac{a}{w} Z_0 \cot\left(\frac{\omega l}{c_0}\right), \quad (5)$$

where a is width of the structure panel, $Z_0 = \rho_0 c_0$ is the characteristic air impedance being $c_0 = 343$ m/s the speed of sound. Thus, the total acoustic impedance of the MS is obtained by $\tilde{Z} = \tilde{Z}_p + \tilde{Z}_c$. Considering the normal incidence of wave, the sound absorption coefficient of the absorber with rigid support can be obtained by

$$\alpha = 1 - \left|\frac{\tilde{Z} - Z_0}{\tilde{Z} + Z_0}\right|^2. \quad (6)$$

Regardless of two or more resonators (HRs) coupled, perfect sound absorption can be achieved mainly by adjusting the parameters d, l and h and consequently the hybrid resonant mode concept can be used so that the average displacement component can be tuned to match the impedance of the medium (air). However, we can also obtain a perfect sound absorption with this meta-structure by converting the incident propagation wave into a sound bound non-radiating surface mode that dissipates energy. Considering the configuration of Figure 2, there is a phase shift π between HRs A and B in relation to the excitation close to the resonant frequency. Thus, the two resonators will have strong responses when the waves from the incident plane reach the meta-structure, but with inverted phase. Since the two HRs are placed close to each other, there will be a strong coupling between them. The coupling of two HRs produces a combined resonant mode where both vibrate significantly with a phase of $\pi = 180^{\circ}$. The distance between the two HRs is much smaller than the incident wavelength and considering the dispersion relation, the transverse or normal wavenumber $k_\perp$ of the reflection wave becomes much larger than the air wavenumber ($|k|_\perp \gg k_{air} = 2\pi/\lambda$). Because ${k_\perp}^2 + {k_\parallel}^2 = {k_{air}}^2$, $k_\perp$ becomes imaginary, being $k_\parallel$ the wavenumber along the surface of the meta-structure. Thus, the reflected wave will become evanescent whose intensity rapidly decays along the normal direction because of a large imaginary $k_\perp$ and consequently the energy is efficiently bound to the absorber.

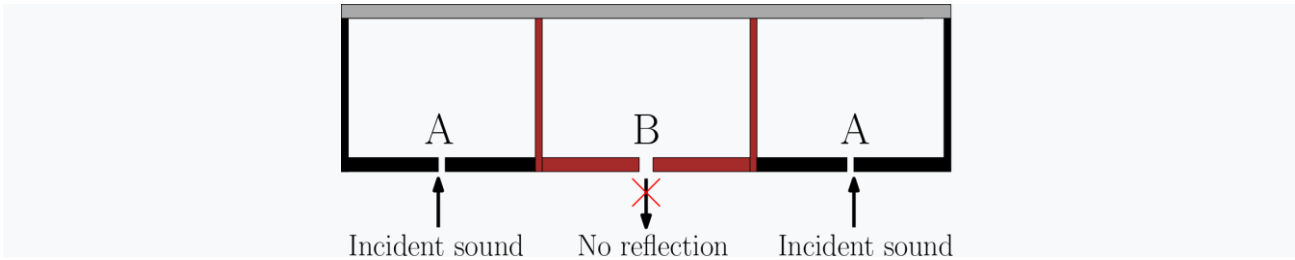

Figure 2. Illustration of the hybrid resonant mode of the meta-structure with two different HRs coupled.

Finite element model and experimental method

To verify the validity of the previous theoretical method, numerical simulations and experiments were carried out. The complete wave simulation by Acoustic-Thermoacoustic interaction in the frequency domain using the finite element (FE) method was performed in the commercial software COMSOL Multiphysics, as shown in Figure 3. The sound absorption curves, sound pressure field, velocity field and energy dissipation were obtained in the simulations. In the FE model, four types of domains are constructed, including the acoustic domain, the thermoacoustic domain for propagating waves in narrow regions (micro-slit), the background pressure field providing a downward incident sound wave, and the perfectly matched layer (PML) for an anechoic boundary. Sound hard boundary is applied to top and to the bottom of the structure. Periodic boundary conditions are applied at the side edges of the absorber. The surface impedance of the MS is calculated by

$$Z_n = \frac{\langle P_n \rangle}{\langle u_n \rangle}, \quad (7)$$

where $\langle P_n \rangle$ and $\langle u_n \rangle$ are the average sound pressure and the average normal velocity of particles on the surface, respectively. Finally, the sound absorption coefficient can be calculated by replacing $\tilde{Z}$ by Z_n in Equation (6).

The experimental performance of the sound absorption coefficient of the absorber samples was carried out in a cylindrical impedance tube with an internal diameter of 107 mm, which corresponds to a plane wave cut-off frequency of 1877 Hz using the standard two-microphone method (ISO 10534-2, 1998), as shown in

Figure 4a. Two different samples were manufactured by the additive fabrication technique of 3D material extrusion using ABS (acrylonitrile butadiene styrene) polymer material. An example of these samples is shown in Figure 4b. The samples were manufactured in a cylindrical shape allowing them to fit perfectly in the internal diameter of the impedance tube. Thus, the spacing allowed for the coupling of four-unit cells of the test sample manufactured and the internal view of the meta-structure, as illustrated in Figure 4b and c, respectively.

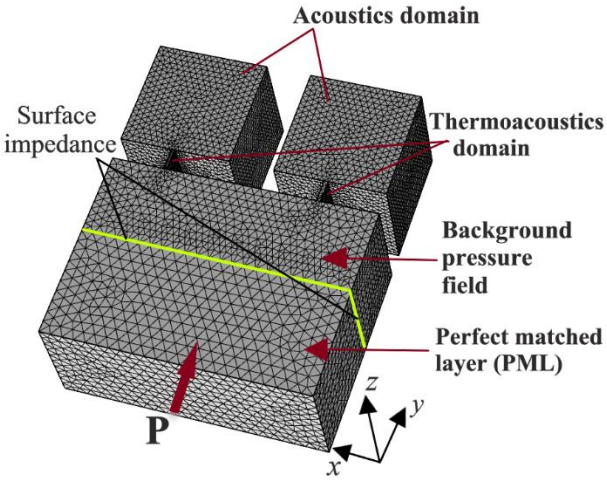

Figure 3. The 3D finite element model of the MS absorber.

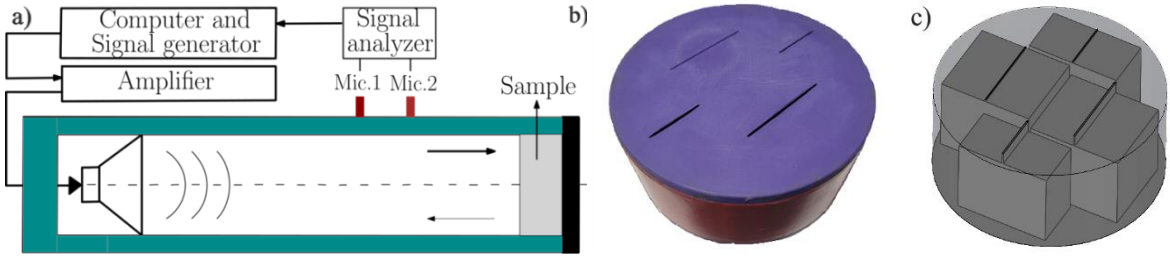

Figure 4. a) Experimental setup to determine the sound absorption of samples. b) Test sample manufactured and c) internal view of the meta-structure.

Results and discussion

In this section, the results of the sound absorption coefficient of the MS are presented. We compare the behavior of the absorber with two different cells coupled, an individual cell, and we explored in detail the physical behavior of the structure. Finally, we present the experimental results and discussions about the energy dissipation. The detailed geometric parameters for the sound absorber with two cells coupled are shown in Table 1.

Table 1. Geometric parameters (in mm) used to manufacture the sound absorber MS.

a	w	l	h	d_A	d_B	H
21	20	20	4	2.0	2.9	24

Figure 5 compares the sound absorption coefficient of the MS for the theoretical model and FE simulation. The blue and magenta dashed lines represent the behavior of individual cells A and B, respectively. F_e in Equation (4) is chosen as 5.2 (the micro-slit used to approach the ellipse has a very high major to minor parameter ratio) and the correction due to the interaction of air radiation in the panel slit ($F(\varepsilon) = 1$), since the panel presents only one perforation. It can be observed that the theoretical model and FE simulation for the coupled absorber present a quasi-perfect sound absorption, and the absorption peaks for the respective methods are located at 1262 Hz and 1263 Hz.

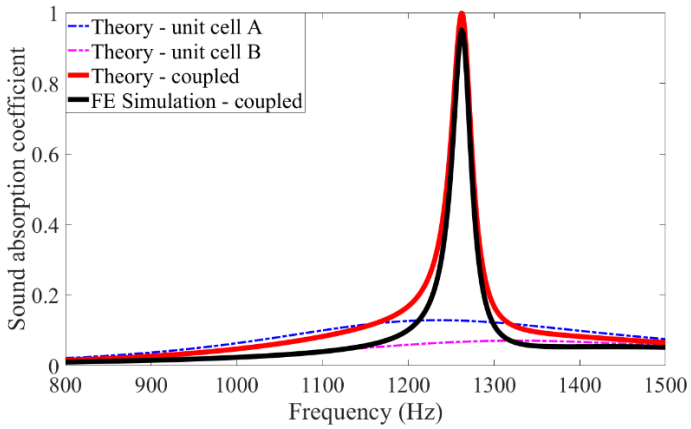

Figure 5. Sound absorption coefficient of unit cells (A and B) and MS with two-resonators coupled.

The sound absorption coefficients for configuration of unit cells A ($d_A = 2.0$ mm) and B ($d_B = 2.9$ mm) individually show peaks around 0.15. These values are much lower than those of the coupled model and this behavior shows the importance of the coupling effect between the two resonators. The sound absorption of the individual cells reduced due to the low acoustic resistance and viscous friction inherent in micro-slits (see Equation (4)). The coupling effect produces a hybrid resonant mode, hence a strong vibration induced by this mode can efficiently potentiate the interaction between acoustic waves and the micro-slits and, consequently, the dissipation of viscous energy since the friction between air and the inner walls of the micro-slit cause dissipation (Zhao et al., 2018).

In Figure 6a we can observe that in the hybrid mode both resonators are strongly excited in the out-of-phase mode at the operating frequency of 1263 Hz. The particle velocity fields indicated by the arrows shows that air particles close to the meta-structure are vibrating parallel to the surface. For the same hybrid mode due to cells resonance, the sound pressure amplitude inside the cavity of the resonators is nine and seven times greater than at the entrance of the panel (micro-slits). As a result, incidence wave energy is dissipated mainly due to increased friction between the acoustic wave and the perforation (Junfei et al., 2016). Furthermore, this behavior is corroborated by the color map of the particle velocity fields in the perforations (see Figure 6b)), whose velocity presents maximum magnitude but with opposite directions.

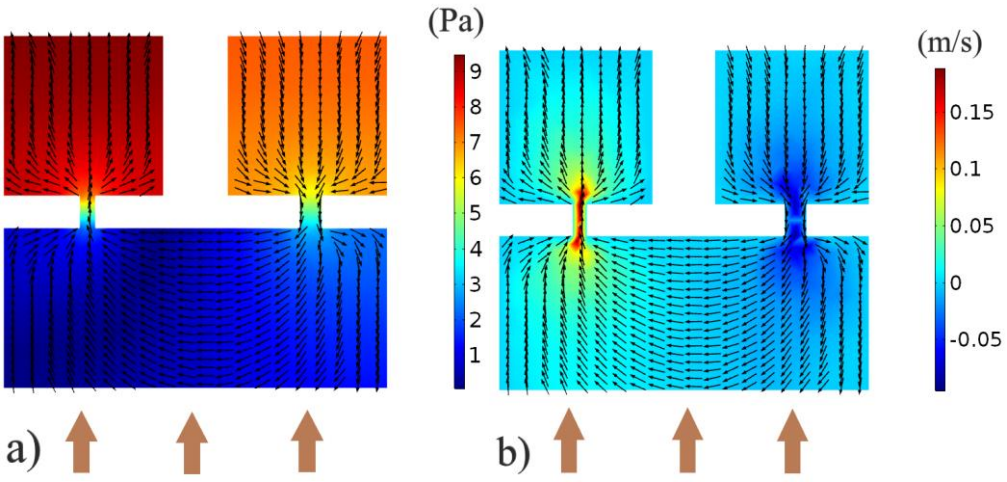

Figure 6. a) Sound pressure and b) particle velocity fields of the MS hybrid resonance mode at operation frequency (1263 Hz).

Figure 7 shows the behavior of the meta-structure consisting of an individual cell with uniform micro-slit ($d_A = 0.38$ mm wide) using the theoretical model and FE simulation. The geometric parameters are listed in Table 1. The theoretical sound absorption (blue solid line) agrees with the simulation (magenta solid line). This behavior confirms the validity of both methods. The 0.38 mm wide micro-slit allows the sound absorption peak (706 Hz) to be much lower than the coupled slits presented previously (1262 Hz). Furthermore, a bandwidth relative to 50% of the maximum absorption is also obtained from 560 Hz to 902 Hz.

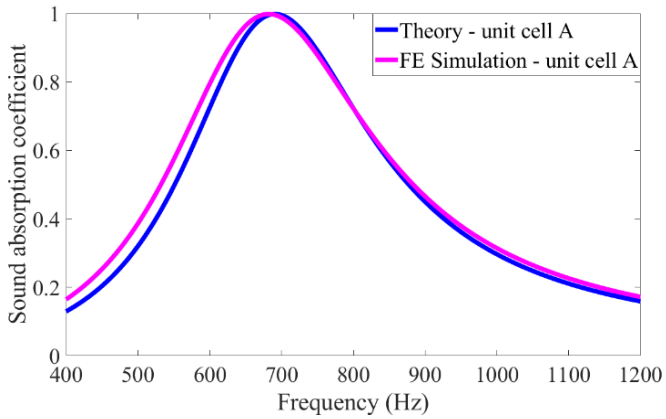

Figure 7. Sound absorption coefficient of the meta-structure with $d_A = 0.38$ mm.

The behavior of the sound absorption coefficient of the meta-structure is strongly dependent on the width (d) and depth (h) of the micro-slit. The influence of these parameters is investigated and shown in Figure 8, the other geometric parameters are fixed and are listed in Table 1. The micro-slit width ranged from 0.2 mm to 1.0 mm while the depth from 1.0 mm to 9.0 mm. Figure 8a shows that the sound absorption presents optimal amplitude, that is, $\alpha \geqslant 0.7$, when the width presents values from 0.23 mm to 0.63 mm. Excellent results ($\alpha \geqslant 0.9$) are achieved between 0.28 mm (f_1 = 609 Hz), 0.40 mm (f_2 = 723 Hz) and 0.48 mm (f_3 = 793 Hz). Furthermore, as this geometric parameter decreases the sound absorption curves gradually move to low frequencies. The influence of depth shown in Figure 8b shows that sound absorption peaks shift strongly towards lower frequencies (from f_4 = 909 Hz to f_5 = 491 Hz) when geometric parameter increases, revealing that this parameter plays a fundamental role in obtaining sound absorption for this frequency region. In addition, shifts in absorption peak to lower frequencies cause only a slight change in the bandwidth at 50% of maximum absorption. This finding can be understood through the cross section of the air cavity that remains unchanged, since the layout of this cavity is not dependent on the *h* parameter.

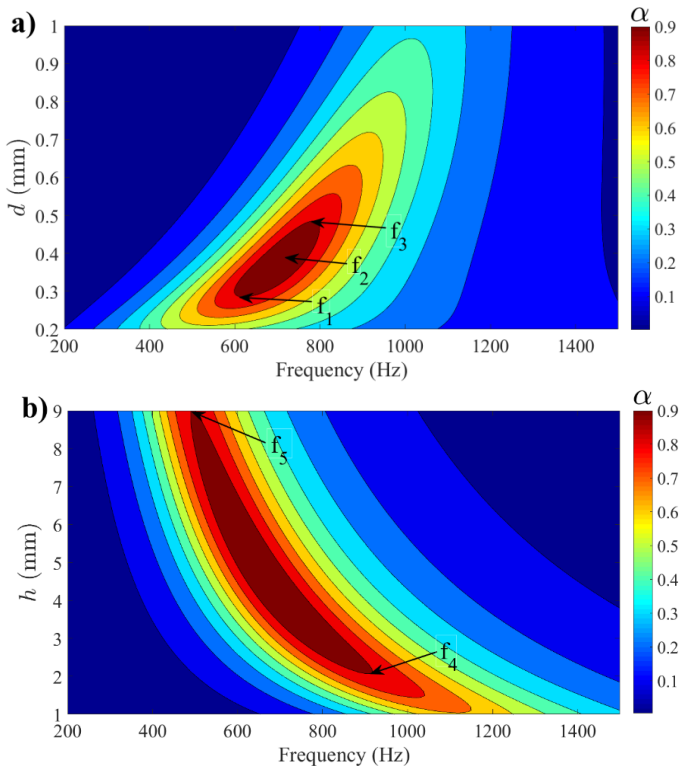

Figure 8. Theoretical behavior of the sound absorption coefficient with variations in the parameters: width (d) and depth (h).

The sound absorption coefficient of the meta-structure was experimentally evaluated in the impedance tube. All samples are composed of two pair of resonators, the geometric parameters used in the manufacture

of the samples are shown in Table 2 and the parameter a (external cavity width) is 46 mm. Due to the limitation of the sample holder of the impedance tube, one of the pairs of sample resonators was manufactured with the height of the smaller resonators, however this difference does not cause major interference in the results.

Table 2. Geometric parameters (in mm) used in the manufacture of meta-structure samples.

Sample	w	l	h	d
1	45	38.6	1.5	0.4
	45	38.6	4.4	0.6
2	43	36.6	0.45	0.32
	43	36.6	3.2	0.56

The theoretical, FE simulation and experimental results of sample 1 are shown in Figure 9. The sound absorption coefficient calculated by the theory model is in good agreement with that obtained by the FE simulation model, where the two peaks with their respective amplitudes are located at 463 Hz (0.99) and 405 Hz (0.99) for theory and 484 Hz (0.99) and 394 Hz (0.99) for the FE simulation. Experimental results are consistent with the prediction results obtained from theoretical model and FE simulation. However, there is a difference caused mainly by not distinguishing between the sound absorption of the peaks, and such difference is due to the accuracy of the 3D printing of sample 1, which is not high enough (± 0.15 mm) and can produce errors mainly in the dimensions of the micro-slits (Almeida et al., 2021a; Zielinski et al, 2020). The peak absorption frequency and amplitude in the experimental results correspond to 436 Hz (0.97). The total thickness of sample 1 is $l + h = 43$ mm, the lowest resonant frequencies are 405 Hz (theory), 394 Hz (FE simulation) and 436 Hz (experimental), and the ratio between the thickness and resonant wavelength at the lowest resonant frequency ($l + h/\lambda$) is less than 5.07, 4.94 and 5.46%, correspondingly, which confirms that the meta-structure operates on the subwavelength scale.

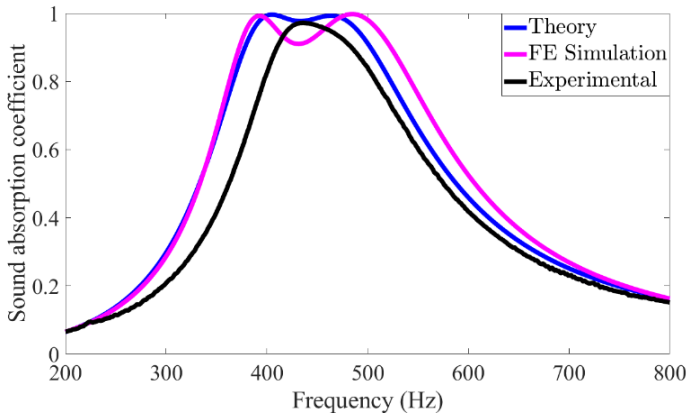

Figure 9. Theoretical, FE simulation and experimental behavior of the sound absorption coefficient for sample 1.

To better understand the behavior of the meta-structure and accurately identify the difference between the sound absorption peaks, the sample 2 is manufactured with a higher resolution (± 0.1 mm). The sound absorption coefficient is reported in Figure 10 and a summary of the basic results is presented in Table 3. In this figure it can be seen that there is good agreement between all the results with the exception of the sound absorption valley at $f_v = 506$ Hz which is smaller in the case of the FE simulation (see Figure 10a). The valley is the lowest because of the weaker resonant coupling in the model. Furthermore, the bandwidths relative to 50% of maximum absorption are 335 Hz (380 Hz to 715 Hz) for theory, 316 Hz (394 Hz to 710 Hz) for FE simulation and 292 Hz (405 Hz to 697 Hz) for experimental.

The total thickness of sample 2 is $l + h = 39.8$ mm, the lowest resonant frequencies are 451 Hz (theory), 443 Hz (FE simulation) and 459 Hz (experimental), thus the ratio between the thickness and resonant wavelength at the lowest resonant frequency ($l + h/\lambda$) is less than 5.23%, 5.14% and 5.32% correspondingly, which confirms that the meta-structure guaranteed low-frequency sound absorption and broadband with the absorber operating at subwavelength scale. The theoretical and experimental behavior of the normalized total acoustic impedance of the meta-structure (see Figure 10b) shows that at peak absorption the real part

presents values close to unity, while the imaginary part approaches zero at two resonant frequencies, which indicates the two absorption peaks (in Figure 10a) showing an approximately optimal fit of the total acoustic impedance of the meta-structure in this medium.

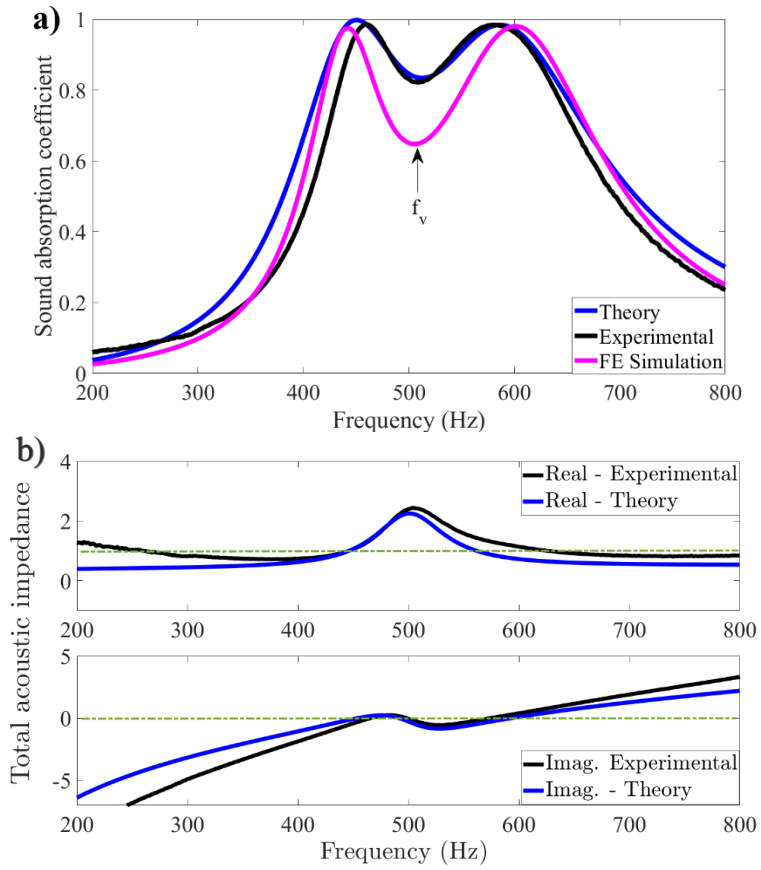

Figure 10. a) Theoretical, FE simulation and experimental behavior of the sound absorption coefficient; b) Theoretical and experimental behavior of the total acoustic impedance for sample 2.

Table 3. Comparison of theoretical, FE simulation and experimental results for sample 2.

Meta-structure (Sample 2)	First peak frequency (Hz)	Second peak frequency (Hz)	First/Second peak sound absorption amplitude
Theory	451	586	0.99/0.98
FE simulation	442	585	0.98/0.98
Experimental	459	600	0.97/0.98

Conclusion

A meta-structure with subwavelength scale was proposed, the absorber provides a broadband sound absorption at low-frequency. Due to the small dimensions of the micro-slits and their strong influence on the behavior of the meta-structure, the resolution used in the manufacturing of the samples must be high (± 0.1 mm) to minimize fabrication errors. This conclusion is important because it is not easy to find detailed and universal information about the 3D printing process, such as tolerance and the minimum thickness. Therefore, the performance and adjust the design of the absorber allow it to be promising candidate for controlling noise.

Acknowledgements

The present research has been supported by the Graduate Program in Mechanical Engineering (POSMEC) and Laboratory of Vibrations and Acoustics of the Federal University of Santa Catarina, Brazil. The authors are grateful for funding from CAPES (Coordination for the Improvement of Higher Education Personnel) of Brazil.

References

Almeida, G. N., Vergara, E. F., Barbosa, L. R., Lenzi, A., & Birch, R. S. (2021a). A low-frequency sound absorber based on micro-slit and coiled cavity. *Journal of the Brazilian Society Mechanical Sciences and Engineering*, *43*(124). DOI: https://doi.org/10.1007/s40430-020-02763-y

Almeida, G. N., Vergara, E. F., Barbosa, L. R., & Brum, R. (2021b). Low-frequency sound absorption of a metamaterial with symmetrical-coiled-up spaces. *Applied Acoustics*, *172*, (107593). DOI: https://doi.org/10.1016/j.apacoust.2020.107593

Almeida, G. N., Vergara, E. F., Barbosa, L. R., Lenzi, A., & Birch, R. S. (2021c). Sound absorption metasurface with symmetrical coiled spaces and micro slit of variable depth. *Applied Acoustics*, *183*, 108312 (2021). DOI: https://doi.org/10.1016/j.apacoust.2021.108312

Cobo, P., & Simón, F. (2019). Multiple-layer microperforated panels as sound absorbers in buildings: a review. *Buildings*, *9*(2), 53. DOI: https://doi.org/10.3390/buildings9020053

Cobo, P., de la Colina, C., & Simón, F. (2020). On the modelling f microslit panel absorber. *Applied Acoustics*, 159, 107118. DOI: https://doi.org/10.1016/j.apacoust.2019.107118

Groby, J.-P., Lagarrigue, C., Brouard, B., Dazel, O., Tournat, V., & Nennig, B. (2015). Enhancing the absorption properties of acoustic porous plates by periodically

embedding Helmholtz resonators. *Journal of the Acoustical Society America*, *137*, 273-280. DOI: https://doi.org/10.1121/1.4904534

Han, L., Ji, H., & Qiu, J. (2021). A broadband sound-absorbing panel based on the coiled coplanar absorber with multiple absorption peaks. *Physica Scripta*, *96*, (085008). DOI: https://doi.org/10.1088/1402-4896/abea30

ISO 10534-2: 1998. (1998). Acoustics - Determination of sound absorption coefficient and impedance in impedance tubes - Part 2: Transfer - function method. Genève, SW: International Organization for Standardization.

Junfei, Li., Wenqi, W., Yangbo, X., Bogdan-Ion, P., & Steven, A. C. (2016). A sound absorption metasurface with coupled resonators. *Applied Physics Letters*, *109*, 091908. DOI: https://doi.org/10.1063/1.4961671

Liu, H., Wu, J. H., & Ma, F. (2021). High-efficiency sound absorption by a nested and ventilated metasurface based on multi-slit synergetic resonance. *Journal of Physics D: Applied Physics*, *54*, (205304). DOI: https://doi.org/10.1088/1361-6463/abe6cd

Ma, G., Yang, M., Xiao, S., Yang, Z., & Sheng, P. (2014). Acoustic meta surface with hybrid resonances. *Nature Materials*, *13*(9), 873-878. DOI: https://doi.org/10.1038/nmat3994

Maa, D. (2000). Theory of microslit absorbers. *Acta Acustica*, *25*(6), 481-485.

Mei, J., Ma, G., Yang, M., Yang, Z., Wen W., & Sheng, P. (2012). Dark acoustic metamaterials as super absorbers for low-frequency sound. *Nature communications*, *3*(756), 1-7. DOI: https://doi.org/10.1038/ncomms1758

Romero-García, V., Theocharis, G., Richoux, O., Merkel, A., Tournat, V., & Pagneux, V. (2016). Perfect and broadband acoustic absorption by critically coupled sub-wavelength resonators. *Scientific Reports*, *6*, 19519. DOI: https://doi.org/10.1038/srep19519

Wei, S., Li, L., Zhigang, C., Linyong, L., & Xiaopeng, F. (2021). A parameter design method for multifrequency perfect sound-absorbing metasurface with coupled Helmholtz resonator. *Journal of Low Frequency Noise, Vibration and Active Control*, *40*(4), 2054-2063. DOI: https://doi.org/10.1177/14613484211019610

Wu, F., Xiao, Y., Yu, D., Zhao, H., Wang, Y., & Wen, J. (2019). Low-frequency sound absorption of hybrid absorber based on micro-perforated panel and coiled-up channels. *Applied Physics Letters*, *114*(15), 151901. DOI: https://doi.org/10.1063/1.5090355

Wang, Y., Zhao, H., Yang, H., Zhong, J., & Wen, J. (2018). A space-coiled acoustic metamaterial with tunable low-frequency sound absorption. *EPL* (*Europhysics*), *120*(5), 54001. DOI: https://doi.org/10.1209/0295-5075/120/54001

Yang, M., Meng, C., Fu, C., Li, Y., Yang, Z., & Sheng, P. (2015). Subwavelength total acoustic absorption with degenerate resonators. *Applied Physics Letters 107*(10), 104104. DOI: https://doi.org/10.1063/1.4930944

Xie, S., Li, Z., Yan, H., & Yang, S. (2022). Ultra-broadband sound absorption performance of a multi-cavity composite structure filled with polyurethane. *Applied Acoustics*, *189*, 108612. DOI: https://doi.org/10.1016/j.apacoust.2021.108612

Zhao H., Wang, Y., Wen, J., Lam, Y. W., & Umnova, O. (2018). A slim subwavelength absorber based on coupled microslits. *Applied Acoustics*, *142*, 11-7. DOI: https://doi.org/10.1016/j.apacoust.2018.08.004

Zielinski T. G., Opiela K. C., Pawlowski P., Dauchez N., Boutin T., Kennedy J., & Groby, J.-P. (2020). Reproducibility of sound-absorbing periodic porous materials using additive manufacturing technologies: round robin study. *Additive Manufacturing*, *36*, (101564). DOI: https://doi.org/10.1016/j.addma.2020.101564